# AVS: A Computational and Hierarchical Storage System for Autonomous Vehicles

Technical Report: CAR-TR-2025-008

Yuxin Wang *University of Delaware* 

Yuankai He *University of Delaware* 

Weisong Shi University of Delaware

#### **Abstract**

Autonomous vehicles (AVs) are evolving into mobile computing platforms, equipped with powerful processors and diverse sensors that generate massive heterogeneous data, e.g., 14 TB per day. Furthermore, supporting emerging third-party applications calls for a general-purpose, queryable on-board storage system. Yet today's data loggers and storage stacks in the vehicles fail to deliver efficient data storage and retrieval. This paper presents AVS, an Autonomous Vehicle Storage system that co-designs computation with a hierarchical layout: modality-aware reduction and compression, hot-cold tiering with daily archival, and a lightweight metadata layer for indexing. The design is grounded with system-level benchmarks on AV data that cover SSD/HDD filesystems and embedded indexing, and is validated on embedded hardware with real L4 autonomous driving traces. The prototype delivers predictable real-time ingest, fast selective retrieval, and substantial footprint reduction under modest resource budgets. The work also outlines observations and the next steps toward more scalable and longer deployments to motivate storage as a first-class component in AV stacks.

#### 1 Introduction

Modern autonomous vehicles (AVs) have effectively become "computers on wheels," integrating heterogeneous sensors with substantial onboard compute to close tight perception—planning—control loops in real time [11]. Over the last decade, milestone systems have solidified this pipeline, as seen in at-scale industry operations by Tesla, Waymo, and all other major companies.

Beyond "driving now," vehicles are increasingly treated as mobile edge compute nodes that support post-drive analytics and services, which is vehicle computing [12]. Many such applications built upon vehicles rely on historical data. Examples include: battery analytics, high-definition (HD) map maintenance, or predictive vehicle maintenance using long-horizon telematics and usage signals.

However, today's production vehicles rarely expose a general-purpose, queryable store for rich historical sensor data. Instead, storage tends to be small and purpose-specific (e.g., event data recorders capture short pre-/post-crash windows like 20s at 10 Hz) [15]. Meanwhile, full-fidelity AV workloads are massive and heterogeneous (e.g., cameras, Li-DAR, radar, GNSS/CAN), amounting to 14 TB/day if logging continuously [25]. And uplinking raw logs is generally impractical: cellular networks and cloud egress costs make bulk offload a non-starter for routine operation, further motivating on-vehicle storage and processing as the AI stack shifts toward in-vehicle edge inference to meet latency, offline availability, privacy, and data-traffic-cost constraints [21].

To follow this shift, this paper makes the following contributions, along with their section roadmap:

- **Storage gap identification.** We identify the on-vehicle storage gap in autonomous vehicles and motivate storage as a first-class AV component (Section 2).
- AVS architecture. We design AVS, a storage-efficient, queryable, compute-hierarchical architecture integrating hot-cold tiering, daily archival, and a lightweight metadata index for predictable real-time ingest and fast selective queries (Section 3).
- Use-guided reduction & compression with system-level evaluation. We develop modality-aware reduction and compression with AV-data-driven benchmarking that links data choices to downstream analytics and retrieval, and evaluate end-to-end on real multi-modal traces across SSD/HDD filesystems and embedded indexing/DBs beyond prior synthetic baselines (Sections 4–5).
- Edge prototype & end-to-end performance. We validate an edge-deployable Raspberry Pi 5 prototype on a real L4 autonomous driving platform with 3 days of driving traces, demonstrating sustained real-time ingest, fast retrieval, and efficient archival under constrained compute (Section 6).

The four key observations and open questions are presented along with each experiment, and the conclusions with implications for AV storage are in Section 7.

# 2 Motivation and Storage Gap Analysis

To motivate our design, 2.1 explains why autonomous vehicles require a storage system for the vehicle computing and what storage patterns it must serve, and then 2.2 surveys why existing logging and edge storage stacks do not meet these requirements.

# 2.1 Vehicle Computing Storage Needs

As shown in Figure 1, traditional vehicle data formed a closed loop: sensor outputs were consumed directly for real-time control. With more powerful computing units and sensors, vehicles are evolving into computing platforms that not only support real-time Autonomous Driving Assistance Systems (ADAS) but also enable data-driven systems or third-party applications that leverage stored logs. This emerging vision of "vehicle computing" treats connected vehicles as platforms for third-party computation and analytics beyond the act of driving [12]. Representative use cases include: (i) infrastructure and mobility analysis, for example, raw multi-vehicle sensor data are transformed into trajectories for traffic reconstruction and planning [26]; (ii) safety, forensics, and policy, which require tamper-evident event logs for reconstruction and liability; (iii) vehicle lifecycle management, like predictivemaintenance models depend on long-horizon telemetry [20]; and (iv) ML pipelines that mine corner cases from historical logs to improve robustness in perception and planning [2] while the current dataset still has limited diversity [28].

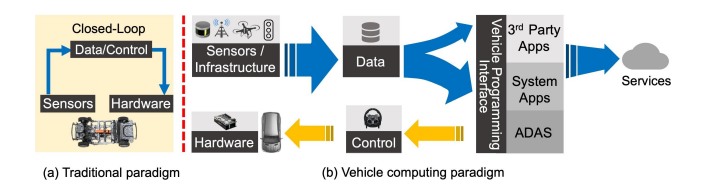


Figure 1: Vehicle computing paradigm.

These applications impose storage requirements that go beyond traditional, ephemeral loggers and are echoed by recent systems perspectives [10]. First, AVs generate massive, heterogeneous data (e.g., high-resolution video, LiDAR, radar, GPS/IMU, CAN), stressing onboard capacity. Second, connectivity is intermittent, making continuous high-bandwidth offload impractical; substantial local storage with intelligent data selection, compression, and prioritization is necessary. Third, retrieval must be flexible: forensics may need seconds around an event, while traffic analytics or model training may require sparse samples over months. These diverse access patterns demand storage layouts and indices that support efficient temporal and modality-selective queries. In short, AVs require robust, scalable, query-friendly on-device storage to serve historical data to the next wave of vehicle data-driven applications.

# 2.2 Storage Systems Gap Analysis

Designing a storage system for AVs exposes shortcomings in today's onboard loggers and edge storage stacks. HydraSpace [24] argues that conventional in-vehicle loggers, built around low-rate CAN telemetry, cannot ingest heterogeneous camera/LiDAR streams at line rate and proposes a multi-layer, compression-centric design. However, HydraSpace focuses on compression within a layered storage architecture and does not deliver a validated in-vehicle logging/indexing pipeline or evaluate continuous ingest of multi-sensor streams.

Standard robotics loggers are also a bottleneck. The ROS bag/MCAP lineage is append-oriented and optimized for offline replay. Recent evaluations show (i) inefficient query performance on large bag/MCAP files, (ii) no support for online queries while a file is actively being written, and (iii) middleware accelerators that improve query performance but are not usable as real-time logging formats [27]. These characteristics explain frequent drops/latency spikes when multiple high-rate sensors are recorded concurrently, independent of raw SSD bandwidth, because the storage format and indexing path, not the device, become the limiting factors.

Beyond these domain-specific limitations, broader research in IoT and cloud/edge storage also reveals persistent gaps. Cai et al. [4] outline a functional framework for IoT-based big-data storage in cloud settings (covering acquisition, management, processing, and mining) aimed at heterogeneous, high-velocity streams. However, their focus remains cloud-oriented and overlooks the lightweight, resource-constrained designs needed on vehicles. More recently, Ferreira et al. [13] survey databases in edge and fog environments, identifying benefits such as reduced latency, improved privacy, and better energy efficiency, while also noting challenges when pushing storage and queries closer to the edge.

While edge storage emphasizes locality and lightweight operation, many leading designs assume networked edge sites with replication and eventual archival to the cloud. Still, these assumptions are untenable inside a vehicle with fixed storage capacity and strict power or thermal budgets. For instance, SEND stores labeled data in network-edge repositories before cloud archival, targeting in-network edge stores rather than single-node, in-vehicle ingest and indexing [16]. FogStore similarly offers geo-distributed access with context-sensitive consistency on top of Cassandra, but relies on replication to meet availability and latency goals, inflating the storage footprint in ways that onboard automotive systems cannot afford [7].

Together, these works underscore that existing IoT, cloud, and edge designs fail to meet the unique constraints of autonomous vehicles, motivating the need for a vehicle-specific storage architecture that balances real-time ingest, resource efficiency, and long-term retention.

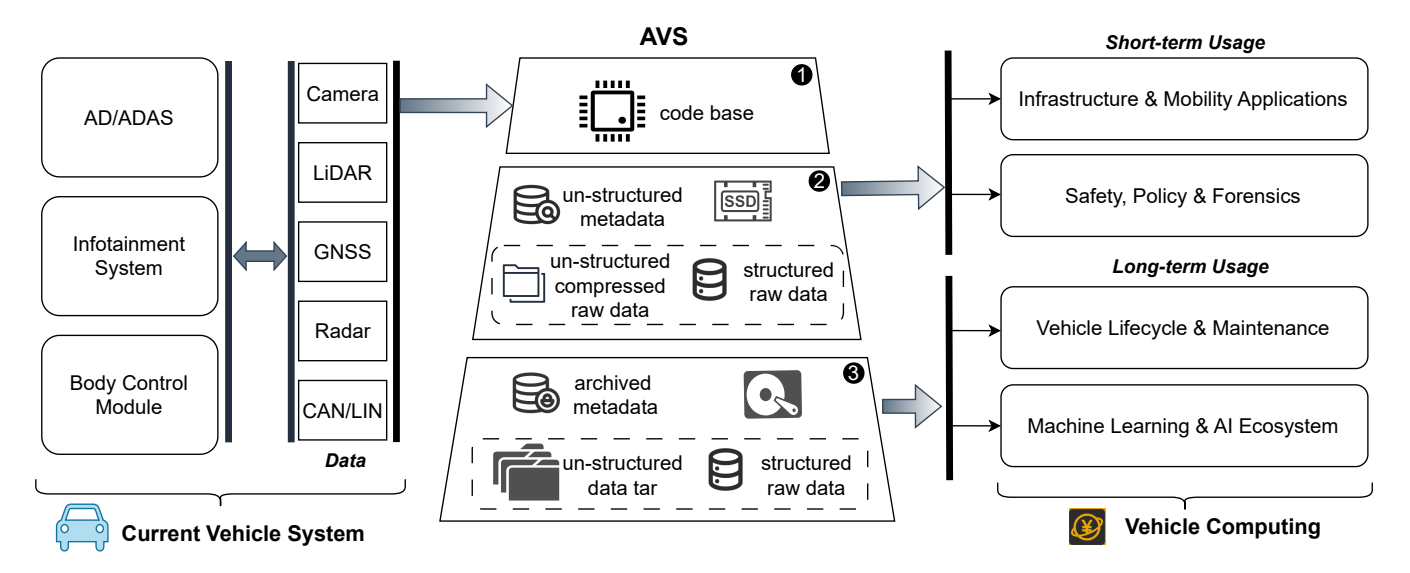


Figure 2: The autonomous vehicle storage system (AVS) architecture.

#### 3 AVS System Architecture

To bridge this gap, we propose AVS, an Autonomous Vehicle Storage system that retains heterogeneous sensor histories and serves diverse downstream uses through four distilled design principles for an in-vehicle storage stack. AVS connects to the autonomous driving stack via an Ethernet switch to receive real-time sensor streams, but it runs on a separate compute unit, which is decoupled from both the AV's main autonomy compute and its operational Electronic Control Units (ECUs). This separation ensures that storage, compression, and indexing activities never interfere with safety-critical perception—planning—control loops while still preserving high-fidelity sensor histories for later retrieval and analytics.

**Design Principles.** A. Heterogeneity-aware ingestion. AV workloads span high-rate LiDAR, multi-camera video, GNSS/IMU telemetry, and low-rate CAN/ECU traces. The system must accommodate different formats and rates concurrently without frame drops, decoupling ingest paths from format-specific bottlenecks observed in ROS bag/MCAP.

- B. Computational and hierarchical storage. AV data is often noisy, and storage on the vehicle is capacity-constrained. Lightweight, streaming-friendly compression reduces footprint, while hierarchical tiers balance line-rate ingest with long-term retention.
- C. Query-friendly organization. Beyond replay, AV applications require selective access, such as per-modality retrieval (e.g., only GNSS), temporal slices (e.g., 5 s around an incident), or sparse sampling across weeks. Flat, append-only blob formats are insufficient; metadata indices and structured layouts must support efficient lookup.
- D. Lightweight, real-time, and resource-aware. AV compute platforms operate under strict thermal and power budgets. Storage components like compression, indexing, and archival

must therefore be streaming-oriented, lightweight, and carefully matched with filesystem and database choices. This ensures predictable performance at line rate without exhausting CPU or memory resources.

**System Design.** Figure 2 illustrates the architecture of *AVS*. To avoid perturbing the AV's real-time autonomy stack, AVS runs alongside it as a storage sidecar, bridging sensor sources and downstream data-driven applications. The architecture follows a three-stage pipeline that also represents the data flow in AVS: data is first processed in the real-time computation stage, then written into the SSD for short-term query and access, and finally migrated to the HDD for long-term retention.

- (i) Real-time ingestion layer. This entry point hosts the AVS core services: data reduction, compression, archival movement, and retrieval. AVS selects the streams to persist, applies reduction and compression to the data accordingly, and then flushes them to the SSD. During vehicle idle periods (e.g., overnight), the archival mover transfers older data from SSD to HDD. The retrieval service provides interfaces for applications to access the most recent history with predictable latency.
- (ii) Hot tier (SSD). The SSD holds the most recent and frequently accessed data and is optimized for line-rate ingest and fast reads via the retrieval interface. To minimize footprint while preserving queryability, AVS stores different data types differently. Unstructured data (e.g., images, LiDAR) is reduced and compressed by the ingestion layer, then written into type-specific directories organized by day. In parallel, a metadata database records each object's attributes (e.g., sensor ID, timestamp) and file path for efficient lookup. Structured data (e.g., GPS, CAN) is written directly into per-day databases under their sensor folders.
  - (iii) Archive tier (HDD). The HDD provides cold archival

for longer on-board retention. Its layout mirrors the SSD but is organized hierarchically by year/month (YYYY/MM) to avoid oversized directories. An archival metadata database logs, for both unstructured and structured datasets, when and where each item was moved, maintaining consistency between hot and cold tiers. To align with HDD sequential I/O, unstructured files are first packed into tar archives before transfer. This reduces fragmentation, improves scan throughput, and enables long-term retention within a fixed onboard storage footprint.

Beyond the overall architecture, AVS enforces three practical requirements <sup>1</sup>. (i) Real-time reduction and compression. Each data stream is reduced, compressed, and persisted to the SSD within a single message period (i.e., before the following message arrives), while preserving task utility for downstream applications. See Section 4. (ii) Filesystems for endurance and throughput. SSD/HDD choices and tuning should minimize fragmentation and write amplification, and support high-rate sequential ingest with fast reads. (iii) Query-friendly metadata and database. The metadata engine must add minimal overhead and support efficient commits and lookups (e.g., batched inserts; range queries by sensor ID and timestamp) to deliver low-latency retrieval. These two system-level benchmarks appear in Section 5. After integrating these details into the proposed architecture, the final end-to-end prototype is presented in Section 6.

# 4 Computational Design: Reduction and Compression

Autonomous vehicles generate massive volumes of sensory data, often several terabytes per day. Storing all raw data is neither efficient nor necessary, as much of it is redundant or irrelevant for future use. Among all sensor modalities, LiDAR and image data dominate the storage footprint. The following sections introduce data reduction and compression tailored for these modalities and evaluate their utility using representative algorithms from downstream applications.

#### 4.1 Data Reduction

# A. LiDAR Data Downsampling

Modern LiDAR sensors produce dense point clouds at high frequency, typically 10 to 20 Hz, with each scan covering a 300 m radius and generating over 2 million 3D points. Continuous storage of raw LiDAR data quickly becomes unsustainable due to both size and redundancy.

For downstream applications involving spatial reasoning or scene reconstruction, raw point density is less critical than the preservation of salient geometric features. Excessive points often introduce unnecessary noise and increase computational and storage overhead without improving algorithmic performance

Among all the LiDAR preprocessing techniques [1], voxel grid downsampling is a widely used lightweight real-time method that reduces point density while maintaining global structure [17]. It divides 3D space into a uniform grid of voxels with edge length r, and within each voxel, only one representative point is retained, typically the centroid. Given a point cloud  $\mathcal{P} = \{\mathbf{p}_1, \dots, \mathbf{p}_N\}$ , the output for each voxel v is:

$$\mathbf{p}_{v} = \frac{1}{|v|} \sum_{\mathbf{p}_{i} \in v} \mathbf{p}_{i} \tag{1}$$

To assess how voxel-based LiDAR downsampling affects geometric processing, we conducted experiments on 11 sequences of the KITTI odometry dataset [5], a widely used benchmark with synchronized LiDAR scans and ground-truth poses from urban driving. We selected KISS-ICP [22] as a representative backend for downstream tasks, such as localization and mapping, due to its robustness, scan-matching architecture, and fully automated configuration (i.e., no manual tuning or ground segmentation). We run the raw scans on KISS-ICP to get the baseline, then apply voxel sizes from 0.1 m to 1.0 m and re-run the pipeline. The goal was to quantify how much point density could be reduced while preserving odometry accuracy.

**Evaluation Metrics:** Two trajectory-based metrics during this experiment were used to quantify performance degradation due to downsampling. Absolute Trajectory Error (ATE) measures the root mean square error (RMSE) between the estimated and ground-truth positions over the whole trajectory. Another is Average Rotation Error (ARE), which measures the average angular deviation (in degrees per meter) between estimated and ground-truth poses. Additionally, the average data size per frame was recorded to analyze the relationship between geometric fidelity and storage reduction. And the processing latency was also considered.

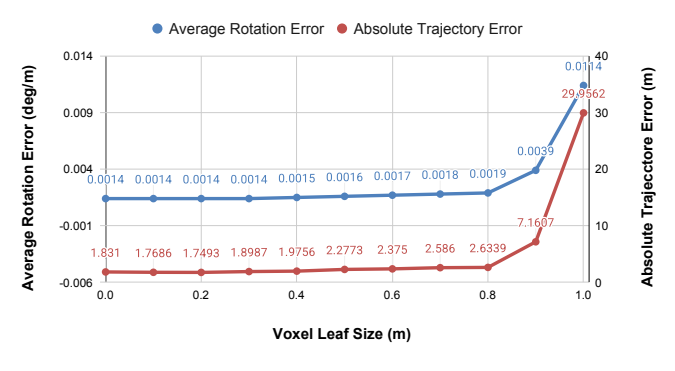


Figure 3: KISS-ICP performance. Red line: Absolute Trajector Error (baseline is 1.831 m). Blue line: Average Rotation Error (baseline is 0.0014 deg/m)

<sup>&</sup>lt;sup>1</sup>Experiment results consistency: Unless otherwise noted, numeric values are rounded to two decimal places. Length values in Tables 2, 4, 7, and 11 are reported to four decimal places for better comparison.

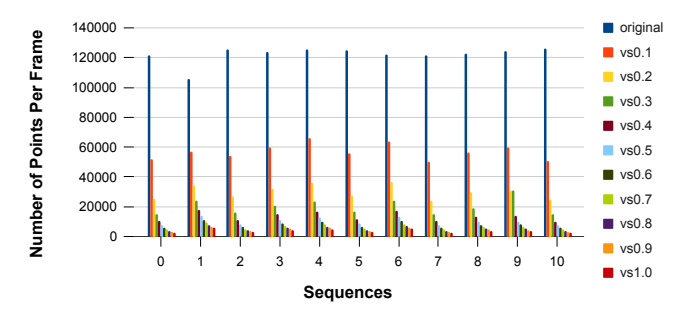


Figure 4: Number of points per frame comparison for different voxel leaf sizes and sequences. (Larger voxel leaf size, more aggressive data reduction)

Table 1: Comparison of Lidar sequences before and after 0.2 m filtering.

Seq.	# Points	# Points / Frame		Size (MB)	Ratio	File Size Keep (%)	Latency (ms)
ocq.	Before Filtered Before Filtered		The Size Reep (70)	Latency (IIIs)			
0	121494	25155	8800	1800	4.83	20.45%	9.18
1	105682	34543	1900	609	3.06	32.03%	8.48
2	125620	26663	9400	2000	4.71	21.28%	9.48
3	123971	32277	1600	414	3.84	25.86%	9.74
4	125718	36271	545	157	3.47	28.86%	10.17
5	125038	27679	5500	1200	4.52	21.82%	9.62
6	122300	36748	2200	647	3.33	29.42%	9.33
7	121331	24297	2100	428	4.99	20.38%	9.23
8	122594	29744	8000	1900	4.12	23.75%	9.64
9	124384	31061	3200	791	4.00	24.71%	9.20
10	125910	24557	2400	472	5.13	19.66%	8.70
Avg.	122186	29909	4150	947	4.20	24.38%	9.34

Figures 3 and 4 show that larger voxels monotonically reduce points and file size, with ATE/ARE remaining flat up to 0.3m. Beyond 0.4m, accuracy begins to degrade; at 1.0m the pipeline fails (ATE 29.96m, ARE 0.0114 deg/m). Most savings come from 0.1 and 0.2m, after which returns diminish while odometry worsens.

At a leaf size of 0.2 m, voxel downsampling gives the best accuracy—size trade-off: average points per frame drop from 122,186 to 56,858 ( $\approx$  53%), while LiDAR odometry quality is preserved given ATE 1.7493 m vs. baseline 1.831 m and ARE unchanged at 0.0014 deg/m. Storage falls to 24.38% of the original ( $\approx$  4.2× reduction), with per-sequence keeps of 19.66% to 32.03%. Table 1 reports actual on-disk folder sizes for .bin frames, the point-reduction ratio (KITTI original  $\div$  filtered), the size-keep percentage, and the average perframe downsampling latency. Overall, a 0.2 m grid maintains geometric fidelity for KISS-ICP while delivering substantial footprint cuts and fast processing within the real-time budget (100ms for Lidar data generation).

#### **B.** Image Frame Deduplication

Unlike LiDAR sensors, cameras mounted on autonomous vehicles typically capture images at much higher rates, often 30 frames per second or more. These image streams are primarily used for object detection and semantic understanding.

However, in practical driving scenarios, especially when the vehicle is stationary or moving slowly (e.g., at traffic lights, in stop-and-go traffic, or during parking), consecutive frames often exhibit minimal change.

As a result, storing every image frame in such scenarios is both redundant and inefficient. Multiple frames collected within the exact second may contain near-identical visual content, offering no additional value for future analysis. For downstream tasks such as incident reconstruction, map annotation, or dataset generation, only a small subset of temporally distinct keyframes is typically sufficient to represent the scene.

To address temporal redundancy in video frames, we apply perceptual hashing (pHash) to identify and discard visually similar frames based on their content [29]. Unlike traditional hashes that capture exact pixel values, pHash generates a compact signature that reflects structural and frequency-domain characteristics, making it robust to minor visual variations such as illumination changes or small shifts in scene composition.

The input image is first converted to grayscale and resized to a fixed dimension (typically  $32 \times 32$ ). A Discrete Cosine Transform (DCT) is then applied to obtain a frequency-domain representation. From the resulting DCT matrix, the top-left  $8 \times 8$  block representing the lowest frequencies is extracted. The mean of these 64 coefficients (excluding the DC component) is computed, and a binary hash is generated by comparing each coefficient  $c_i$  to the mean  $\mu$ :

$$h_i = \begin{cases} 1, & \text{if } c_i \ge \mu \\ 0, & \text{if } c_i < \mu \end{cases} \tag{2}$$

This yields a 64-bit binary vector as the perceptual hash of the image. Visual similarity between two images is quantified using the Hamming distance between their hashes:

Hamming
$$(H_1, H_2) = \sum_{i=1}^{64} 1(H_{1,i} \neq H_{2,i})$$
 (3)

If the Hamming distance is below a predefined threshold, the newer frame is deemed a duplicate and discarded.

To determine the optimal Hamming distance for preserving temporal and semantic information in downstream perception tasks, we evaluate with CenterTrack, a joint 2D detection—tracking framework robust to frame skipping and occlusion that leverages adjacent-frame motion cues [30]. Experiments are conducted on the KITTI Tracking dataset (21 sequences, 10 Hz).

We first establish a baseline by running CenterTrack on the original, unfiltered image streams. Next, we apply perceptual hashing (pHash) with Hamming distance thresholds in 2,6,10 to progressively remove visually redundant frames. The filtered sequences are re-evaluated using the unchanged model, and deviations from the baseline quantify the impact of deduplication on multi-object tracking quality.

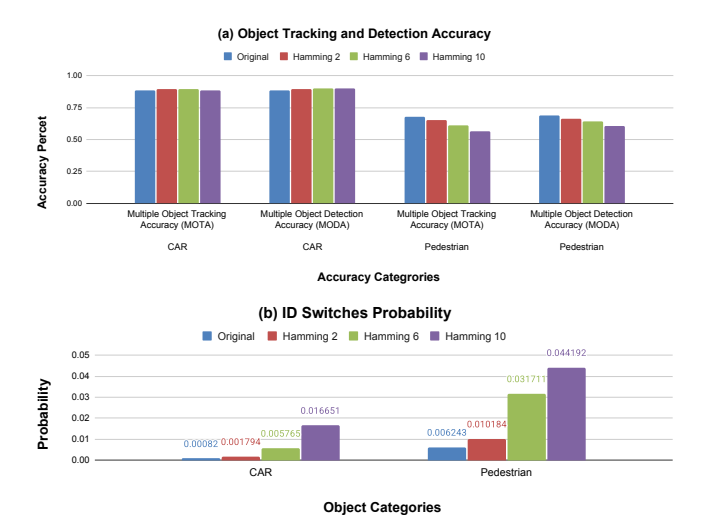


Figure 5: CenterTrack performance with different deduplication settings. (a) Shows multiple object tracking and detection accuracy for cars and pedestrians (the larger the better). (b) Shows ID switches probability for cars and pedestrians (the smaller the better)

**Evaluation Metrics:** The three key metrics are used for tracking performance analysis. Multiple Object Tracking Accuracy (MOTA) serves as a comprehensive indicator that captures false positives, missed detections, and identity switches in a single score, reflecting the overall reliability of the tracking system. Multiple Object Detection Accuracy (MODA) focuses specifically on detection quality, measuring how well the algorithm identifies and localizes objects regardless of identity tracking. Finally, the number of ID switches provides insight into the consistency of object identities across frames, with fewer switches indicating more stable and coherent tracking.

In addition to these accuracy-related metrics, we also record the average number of frames per sequence after deduplication to quantify the reduction ratio, and we measure processing latency to assess the practicality of the method for real-time usage.

The CenterTrack performance and data reduction ratio results are shown in the Figure 5-6,

Across Figure 5 (a–b), car detection/tracking is invariant mainly to frame pruning, while pedestrian quality degrades with higher dedup levels. This asymmetry aligns with object scale and motion: cars are larger, closer, and move more predictably, so occasional frame removal does not break Center-Track's temporal linking; pedestrians are smaller, often distant or occluded, and exhibit fine, irregular motion, so subsampling erodes the short-term cues needed to maintain identity, which is reflected in rising ID switches.

With a conservative threshold ( $\tau$ =2), deduplication makes a 28.25% reduction shown in Figure 6, with an average 2.2 ms/frame real-time processing latency within a 100ms bud-

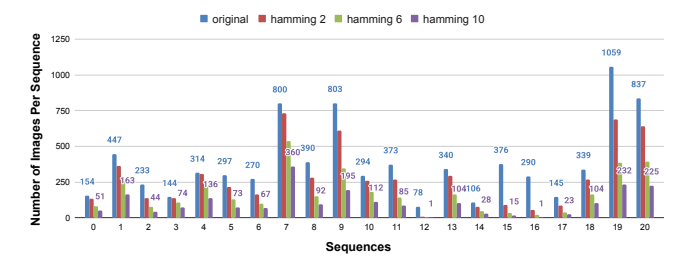


Figure 6: Number of images per sequence under different hamming distance settings.

get. Vehicle tracking slightly improves as redundant frames are pruned, while pedestrian tracking shows modest declines under tighter temporal sampling. This highlights that pHash-based deduplication yields significant storage savings with minimal compute cost but may require adaptive thresholds in pedestrian-heavy settings.

# 4.2 Data Compression

#### A. LiDAR Point Cloud Compression

There are two widely used methods for the point cloud compression: octree-based compression provided by PCL for .pcd files, and LASzip compression for .las files (producing .laz outputs).

PCL's **octree compression** recursively partitions the point cloud space into voxels using an octree data structure [17]. Within each voxel, point positions are quantized and encoded relative to their local voxel centroid. Compression effectiveness can be tuned by adjusting the octree resolution (i.e., leaf size), trading off geometric fidelity for storage gain. High-resolution settings preserve more spatial detail, while lower-resolution settings yield better compression ratios by coarsely representing local geometry.

The **LASzip** algorithm used to compress .las files to .laz leverages entropy coding and predictive modeling techniques tailored to LiDAR data [8]. It compresses coordinate deltas, intensity values, and other fields using arithmetic coding and context models. LASzip achieves high compression ratios without loss of precision, making it suitable for long-term archival or cloud-based storage. However, it will have more complex computation.

The objective of this experiment is to identify the LiDAR compression method that can achieve real-time compression and writing, maintain a high compression ratio, and minimize decompression error. We compare LiDAR compression schemes including Octree (low/medium/high resolution) and LAZ on 11 KITTI sequences, the **evaluation metrics** include compression ratio (original .bin file size ÷ compressed file size), bits per point (bpp), average nearest neighbor (NN) distance for decompression error, and compression/decompression latency; average results are in Fig-

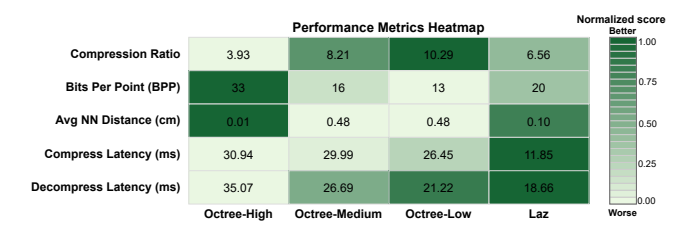


Figure 7: Lidar compression benchmark results. (Compression ratio and BPP larger is better, Avg NN Distance, compress and decompress latency, smaller is better)

Table 2: The KISS-ICP average performance over 11 KITTI LiDAR sequences: KITTI vs. VS0.2 vs. LAZ.

Metrics	KITTI	VS0.2	LAZ
Average Translation Error (%)	0.5164	0.5121	0.5136
Average Rotation Error (deg/m)	0.0014	0.0014	0.0014
Absolute Trajectory Error (m)	1.8310	1.7493	1.7486
Absolute Rotation Error (rad)	0.0801	0.0582	0.0571
Average Frequency (Hz)	85.2727	94.3636	106.9091
Average Runtime (ms)	12.6364	11.7273	10.6364

ure 7. Although low/medium Octree achieves competitive compression ratios, it incurs larger geometric error (average nearest-neighbor distance, ANN-D) than LAZ and higher encode/decode latencies; high-resolution Octree further worsens speed without clear fidelity gains. Overall, LAZ offers the best balance of real-time viability, footprint reduction, and geometry preservation.

To verify downstream fidelity, we run KISS-ICP on three inputs with each of 11 KITTI sequences: original point clouds, voxel-downsampled clouds (leaf 0.2 m), and LAZ-compressed-then-decompressed clouds after the same downsampling with the same **evaluation metrics** used in section 4.1. As shown in Table 2, LAZ-decompressed performance closely matches both original and downsampled inputs, indicating negligible impact on odometry quality. In practice for AVS, PCD is preferable when prioritizing a small-on-disk but fast-to-read format (only slightly larger than BIN), while LAZ is the choice when maximizing SSD efficiency, with strong geometric fidelity being paramount.

#### **B.** Image Compression

The most common image formats used in AV datasets such as KITTI, nuScenes [3], and Waymo Open Dataset [18] are JPEG (.jpg) and PNG (.png), with WebP increasingly adopted in cloud applications due to its efficient coding. Choosing the optimal image format onboard is crucial for balancing compression ratio, latency, and retained perceptual quality, particularly when images are later used for tasks such as semantic understanding or dataset curation.

Each image format relies on distinct compression princi-

ples. **JPEG** is based on the discrete cosine transform (DCT), which transforms an image from the spatial domain into the frequency domain [23]. Specifically, for an  $N \times N$  image block, the DCT is computed as:

$$F(u,v) = \frac{1}{\sqrt{2N}}C(u)C(v)\sum_{x=0}^{N-1}\sum_{y=0}^{N-1}f(x,y)\cos\left[\frac{(2x+1)u\pi}{2N}\right] \times \cos\left[\frac{(2y+1)v\pi}{2N}\right]$$
(4)

where f(x,y) is the pixel intensity at spatial coordinates (x,y), and  $C(u)=\frac{1}{\sqrt{2}}$  when u=0, otherwise C(u)=1. The resulting coefficients F(u,v) represent frequency components, which are quantized using a perceptual quantization matrix to reduce less noticeable high-frequency components. This quantization step introduces lossy compression, the degree of which is controlled by a quality parameter (commonly ranging from 0 to 100).

**JPEG 2000**, by contrast, uses the discrete wavelet transform (DWT) instead of DCT [19]. The DWT decomposes the image into a hierarchy of sub-bands with different spatial resolutions, using a series of high-pass and low-pass filters followed by downsampling. Mathematically, the 1D DWT of a signal f(n) can be expressed as:

$$A_{j+1}(n) = \sum_{k} g(2n-k)a_j(k), \quad D_{j+1}(n) = \sum_{k} h(2n-k)a_j(k)$$
(5)

where g and h are low-pass and high-pass filters, respectively, and  $A_j(n)$  and  $D_j(n)$  are the approximation and detail coefficients at level j. This multi-scale decomposition enables more localized and energy-efficient representation of image content, yielding higher compression efficiency and improved reconstruction at lower bitrates compared to JPEG, but at the cost of increased computational complexity and encoding time.

**WebP** combines elements of DCT-based intra-frame prediction with entropy coding techniques derived from the VP8 video codec [6]. It predicts pixel blocks from neighboring blocks, then encodes residuals using variable-length codes and context-adaptive binary arithmetic coding. Its hybrid approach often results in better compression efficiency than JPEG for similar perceptual quality, although encoding latency can vary based on implementation and hardware acceleration.

We benchmark four formats, JPEG (quality 85 and 95), JPEG 2000 (target ratio 1:500), WebP (quality 90), and the original PNG baseline on 21 KITTI sequences. **Evaluation Metrics** include compression latency in milliseconds (from initiating a cv::Mat write to physical flush), compression ratio (PNG size ÷ encoded size), and downstream tracking

Table 3: Comparison of image compression. (Reported numbers are averaged across 21 KITTI image sequences.)

Metrics	JPEG (85)	JPEG (95)	JPEG2000	WebP
Compression Time (ms)	1.19	1.45	95.39	34.61
Compression Ratio	7.70	4.06	1.12	6.83

Table 4: CenterTrack performance for car and pedestrian under hamming 2 deduplication with different compression settings. (Baseline is hamming 2 deduplication results.)

Object	Setting	MOTA	MODA	ID-switches
	Hamming 2	0.8935	0.8953	0.0018
Car	Hamming 2 + JPG 85	0.8909	0.8935	0.0026
	Hamming 2 + JPG 95	0.8952	0.8972	0.0020
	Hamming 2	0.6506	0.6608	0.0102
Pedestrian	Hamming 2 + JPG 85	0.6463	0.6600	0.0137
	Hamming 2 + JPG 95	0.6533	0.6635	0.0102

quality (Sec. 4.1) using CenterTrack. Table 3 shows that JPEG offers the lowest latency and balanced compression; WebP provides a relatively balanced speed—size trade-off; JPEG 2000 incurs the highest latency with only modest ratio gains under default (visually lossless) settings. Given KITTI's  $10\,\mathrm{Hz}$  rate, real-time writing requires  $< 100\,\mathrm{ms}$  per frame; this favors low-latency codecs, so we further analyze different JPEG qualities. Using the deduplicated streams (Hamming threshold 2) for consistency, Table 4 summarizes CenterTrack performance: quality 85 yields a slight accuracy dip, while quality 95 preserves nearly all baseline performance, yet still achieves a  $4.06\times$  size reduction with  $1.45\,\mathrm{ms}$  per-image latency. Balancing storage efficiency, write-time constraints, and downstream robustness, we adopt JPEG at quality 95 as the default SSD format.

Observation 1: Data redundancy. AVS reduces footprint by compression, pruning near-duplicate frames, and downsampling LiDAR point clouds, while preserving tracking and localization accuracy. The impact of these reductions on task accuracy follows the thresholds shown in Figure 3 and Figure 5. Here, "redundant" is workload-coupled: successive images or scans that are visually or geometrically similar within short horizons add little value for replay or map refresh. Open questions include: how to set thresholds adaptively (e.g., scene motion or entropy-aware rather than fixed Hamming/error bounds)? How can we safeguard rare events (e.g., trigger windows around anomalies) to prevent pruning from harming forensics or retraining? Additionally, how can we schedule deduplication and compression to cap peak CPU/RSS on the hot tier? And how to make pruning decisions auditable (metadata/provenance) so downstream analytics can reason about what was kept vs. dropped?

# 5 Low-level System Selection

This section focuses on system-level storage optimization, specifically targeting unstructured, high-volume data from Li-DAR point clouds and camera images. We evaluate file system and database configurations across the hot (SSD) and archive (HDD) tiers to ensure efficient write throughput, minimize flush latency, and extend storage media lifespan.

# 5.1 Filesystem Choosing and Benchmark

The choice of filesystem plays a crucial role in the performance and reliability of AVS. In our design, we benchmark two widely used Linux filesystems—EXT4 and XFS—on both SSD and HDD storage tiers. EXT4 is the most common and stable Linux filesystem, known for its reliability and compatibility across various workloads. XFS, in contrast, is a high-performance, scalable filesystem optimized for handling large files and heterogeneous datasets. These two filesystems were selected for benchmarking due to their widespread adoption, contrasting design philosophies, and balanced reliability and IO performance [9, 14], which make them suitable candidates for different tiers of a hierarchical storage system.

**EXT4** (Fourth Extended Filesystem) is a journaling filesystem that improves upon its predecessor, EXT3, with features such as delayed allocation, multiblock allocation, and extents. These optimizations enhance both read and write throughput while maintaining backward compatibility. EXT4 is particularly well-suited for general-purpose workloads and real-time data logging due to its stable metadata handling and relatively low write amplification.

XFS is a high-performance 64-bit journaling filesystem designed for parallel I/O operations, large files, and scalable storage systems. It uses extent-based allocation and aggressive metadata prefetching, which reduces fragmentation and improves sequential I/O performance. XFS is particularly effective for workloads that involve large, continuous data streams or require efficient access to massive datasets—making it a strong candidate for archival storage tiers.

In the proposed hierarchical AVS design, the SSD tier serves as the primary buffer for incoming raw sensor data. It must support high-frequency real-time writes and allow efficient random access for downstream applications (e.g., searching for specific visual events over the past week). Therefore, the SSD filesystem must offer: Low write synchronization latency, high random read performance, and low write amplification to preserve SSD endurance.

The HDD tier, by contrast, functions as a cold archive for long-term storage. Here, the primary requirements are: High sequential write and read throughput for efficient bulk data transfers and low fragmentation to maximize usable storage space and read efficiency.

The experiment pipeline is illustrated in Figure 8. In our setup, the SSD is the first stage of the data logging system,

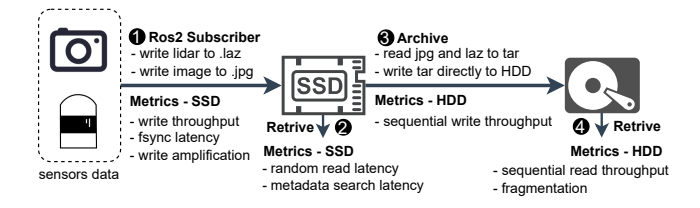


Figure 8: File system benchmark experiment logic.

where a ROS2 subscriber continuously receives LiDAR and camera data streams. LiDAR point clouds are stored in compressed .laz format, while images are stored as .jpg. For each file written to the SSD, we measure write throughput, fsync latency, and write amplification, which reflect the ability of the SSD to handle real-time sensor logging workloads.

Next, a file parser sequentially reads the .jpg and .laz files from the SSD, aggregates them into a single tar archive, and transfers this archive to the HDD. During this stage, we record the HDD write throughput, which represents the effective pipeline performance when migrating logged data to archival storage.

For the SSD retrieve analysis, to capture metadata overhead and latency under random access conditions, we implement a random reader that selects 500 .jpg and 500 .laz files at random from the SSD and measures 4 KiB random read latency and metadata search latency.

Finally, the sequential reader evaluates HDD performance by reading the complete tar archives back from disk. At this stage, we calculate HDD sequential read throughput as well as file fragmentation, measured using the metric:

$$frag\_index = 1 - \left(\frac{largest\_extent\_bytes}{total\_file\_size\_bytes}\right)$$
 (6)

This captures the extent to which files are split across noncontiguous regions of the HDD.

The experiments were performed on the KITTI dataset with 21 image sequences and 11 LiDAR sequences. Identical datasets were applied across both EXT4 and XFS filesystems on SSD and HDD for a fair comparison. Each experiment was repeated three times to minimize noise and capture stable average values.

The results are reported in Table 5 and Table 6. For SSD logging, EXT4 and XFS achieve comparable write throughput. Still, XFS provides slightly lower fsync latency and smaller write amplification, making it more efficient when writing many small files with synchronous commits. Sequential read throughput on SSD is also marginally higher under XFS.

More noticeable differences appear on the HDD. XFS consistently delivers higher sequential read and write throughput compared to EXT4, and most importantly, no fragmentation is observed across the entire process. In contrast, EXT4 shows a measurable fragmentation index (approximately 0.66), indicating that large tar archives are not always stored contigu-

Table 5: SSD filesystem benchmark results: EXT4 vs. XFS. (Reported numbers are averaged across 11 lidar sequences and 21 image sequences.)

	EXT4		XFS	
Metrics	.jpg	.laz	.jpg	.laz
Average Write Throughput (MB/s)	2.06	1.00	2.06	1.09
Average fsync Latency (ms)	2.07	1.74	1.94	1.57
Average Write Amplification	1.20	1.38	1.06	1.12
4 KiB Random Read Latency (ms)	4.93	5.27	4.91	5.16
Metadata Search Latency (ms)	0.21		0.20	
Tar file size (MB)	3842.31		3842.31	

Table 6: HDD filesystem benchmark results: EXT4 vs. XFS. (Reported numbers are averaged across 11 lidar sequences and 21 image sequences.)

Metrics	EXT4	XFS
Sequential Write Throughput (MB/s)	103.00	107.49
Sequential Read Throughput (MB/s)	119.11	124.71
Fragmentation (frag_index)	0.66	0.00

ously. This has direct consequences for long sequential reads when replaying or analyzing archived data.

Overall, while SSD performance differences between EXT4 and XFS are relatively small, the advantages of XFS on HDD, which has higher sequential throughput and zero fragmentation, make it a better fit for autonomous vehicle storage pipelines. Considering that real workloads require both real-time logging to SSD and efficient migration to HDD for long-term archival, XFS's characteristics align well with the requirements of large-scale AV data logging systems.

Observation 2: Filesystem patterns. AV ingest is appendheavy with durable small files and frequent directory/metadata lookups, while replay/analytics favor long sequential reads over archived batches. Thus, filesystem choice primarily affects p99 tails, fragmentation, and device wear. In our experiment, XFS shows better performance under this data pattern. But look ahead, there are some open questions: for the hot tier, to what extent does size and fsync batching policy minimize write latency and write amplification without compromising query freshness? For the cold tier, what archive granularity (hourly vs daily vs multi-day) best limits fragmentation over weeks while preserving peak sequential MB/s? Beyond EXT4/XFS policy, do zone-aware or log-structured file systems yield further gains for this AV workload?

# 5.2 Database Selection and Comparison

In AVS, a lightweight embedded database is used to manage both unstructured metadata (e.g., file paths and timestamps) and structured sensor data (e.g., GPS latitude, longitude, and

Table 7: Comparison of SQLite and RocksDB. (Reported numbers are averaged across three runs, each comprising 1,000 inserts and 1,000 queries.)

Metric	SQLite	RocksDB
Insert latency (ms)	0.0016	0.0053
Query range latency (ms)	0.0098	0.0073
Final DB size (MB)	2.6836	2.7757

altitude). This design supports flexible post-hoc data retrieval while minimizing runtime overhead on resource-constrained edge devices. To meet these requirements, we evaluate two embedded database engines: SQLite3 and RocksDB.

SQLite3 is a widely-used, serverless relational database engine optimized for low-overhead, ACID-compliant workloads. It stores data in a single file and supports rich SQL query semantics with minimal resource usage, making it well-suited for logging applications on embedded systems. RocksDB, in contrast, is a high-performance key-value store based on the Log-Structured Merge-tree (LSM) design. It is optimized for write-heavy workloads and large-scale data ingestion. It supports fast prefix-based range scans, but with a larger storage footprint and more aggressive background compaction behavior.

To evaluate the trade-offs, we implemented a unified benchmarking framework simulating realistic ingestion and retrieval workloads for timestamp-indexed AV data. We recursively scan two sensor data directories, images (.jpg) and LiDAR scans (.laz), where each file is named using a 13-digit millisecond timestamp. All files are indexed into both databases using a standard schema: SQLite uses a composite primary key (type, timestamp) and RocksDB uses lexicographically ordered keys in the format "<type>:<ti>timestamp>".

To benchmark query performance, we construct a shared set of 1,000 range queries, each spanning a ±500 ms window centered on a randomly sampled timestamp. Queries in SQLite use SELECT ... WHERE ts BETWEEN? AND?, while RocksDB performs prefix-bound iterator scans using Seek(start) and stops at end. **Metrics** collected include average insert latency, average range query latency (both in milliseconds), total number of rows scanned, and final database size (MB). All experiments were repeated three times, and the final average results are reported in Table 7.

As expected, RocksDB exhibits lower query latency due to its optimized iterator-based access path. However, this comes at the cost of higher insert latency and significantly larger on-disk footprint due to write amplification and compaction. Given that AVS prioritizes low-overhead logging and only requires eventual (not real-time) access to stored data, SQLite is selected as the default metadata store due to its smaller footprint, lower write latency, and simpler deployment model on embedded platforms.

#### 6 Prototype and Implementation

#### **6.1 System Implementation**

To validate AVS's feasibility and end-to-end functionality, we implemented a complete prototype on a Raspberry Pi 5 with a 256 GB NVMe SSD and a 1 TB WD10SPZX HDD. The Pi 5 integrates a Broadcom BCM2712 SoC (quad-core Arm Cortex-A76 @ 2.4 GHz) with 8 GB RAM, providing a realistic embedded compute envelope. The SSD is partitioned into (i) a system partition for boot and code and (ii) a dedicated 100 GB partition used as the hot tier for real-time ingest and query, while the 1 TB HDD serves as the cold archival tier. Both tiers are formatted with XFS for consistent semantics and performance across the prototype. The resulting storage layout is shown in Figure 9. The prototype is connected to the vehicle via Ethernet, and the hardware setup and connection are illustrated in Figure 11.

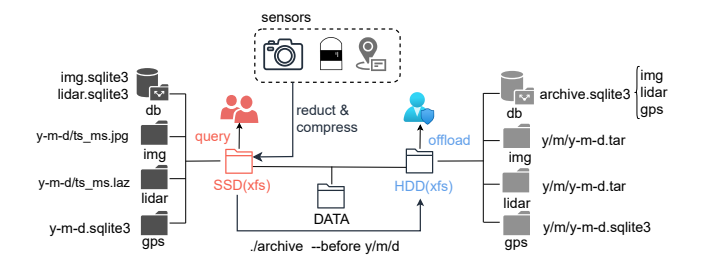


Figure 9: The prototype system structure.

avs	_images & avs_lidar	archive_images	s & _lidar & _gps
sensor_id data_type	TEXT NOT NULL TEXT NOT NULL	sensor_group	TEXT NOT NULL
ts_ms path	INTEGER NOT NULL TEXT NOT NULL	day	TEXT NOT NULL
PRIMARY KE	Y (sensor_id, data_type, ts_ms)	path	TEXT NOT NULL
	avs_gps	start ms	INTEGER NOT NULL
ts_ms	INTEGER PRIMARY KEY	-	
latitude	REAL	end_ms	INTEGER NOT NULL
longitude	REAL	file/row count(for gps)	INTEGER NOT NULL
altitude	REAL	me/row_count(for gps)	INTEGER NOT NOTE
cov_xx	REAL	archived_ms	INTEGER NOT NULL
cov_yy	REAL	sha256 hex	TEXT
COV_ZZ	REAL	SHA250_Hex	IEXI

Figure 10: The schema used for each module in AVS.

For the prototype deployment, the 100 GB SSD partition and HDD are both mounted under a common DATA root. An AVS subscriber pipeline runs on a Raspberry Pi 5, performing real-time image deduplication, lidar downsampling and compression before storing data to the SSD. Unstructured sensor streams are organized by type and day: camera frames are stored as <code>images/YYYY-MM-DD/ts\_ms.jpg</code> and LiDAR scans as <code>lidar/YYYY-MM-DD/ts\_ms.laz</code>. Lightweight metadata indices are maintained in <code>db/avs\_image.sqlite3</code> and <code>db/avs\_lidar.sqlite3</code> to support efficient time-window and sensor-scoped queries. Structured GPS data are recorded

Table 8: Recording performance comparison of AVS and ros2bag under different configurations (sqlite and mcap, raw and zstd). All experiments were conducted with mixed and concurrent sensor stream on a Raspberry Pi 5 equipped with 8 GB RAM and a Broadcom BCM2712 quad-core Arm Cortex A76 processor at 2.4 GHz.

		Workload			NVMe SMART (deltas)			
Day	Method	Data Size (GB)	CPU avg/max (%)	RSS avg/max (MB)	Data Units Written (GB)	WAF	Ctrl Busy (min)	Host Write Commands
	AVS	4.10	86.53 / 105.90	198.94 / 207.45	5.56	1.36	1	184,871
	ros2bag sqlite	35.75	27.53 / 92.20	81.47 / 81.62	37.49	1.05	2	37,920
Day 1 (720s)	ros2bag sqlite zstd	21.53	51.48 / 135.50	96.51 / 99.22	22.58	1.05	1	24,012
-	ros2bag mcap	35.73	15.68 / 170.30	<b>73.97</b> / 76.06	37.12	1.04	1	29,150
	ros2bag mcap zstd	21.50	43.55 / 102.30	99.12 / 101.49	22.58	1.05	1	24,012
	AVS	4.21	93.28 / 113.50	195.58 / 205.84	5.63	1.34	1	179,007
	ros2bag sqlite	33.37	30.83 / 86.10	<b>78.67</b> / 78.78	35.00	1.05	2	31,817
Day 2 (671s)	ros2bag sqlite zstd	19.97	53.82 / 112.90	104.93 / 105.96	20.95	1.05	1	20,242
	ros2bag mcap	33.38	16.97 / 96.20	78.70 / 80.62	35.00	1.05	2	27,839
	ros2bag mcap zstd	19.89	44.98 / 179.00	119.54 / 124.11	20.87	1.05	1	16,979
	AVS	3.70	88.39 / 107.40	206.75 / 210.82	4.95	1.34	1	168,632
	ros2bag sqlite	32.31	27.92 / 169.80	76.82 / 76.91	33.88	1.05	1	30,353
Day 3 (648s)	ros2bag sqlite zstd	18.10	51.76 / 200.20	115.17 / 117.46	18.98	1.05	1	16,541
	ros2bag mcap	32.27	<b>15.57</b> / 96.20	<b>74.05</b> / 76.12	33.84	1.05	1	26,458
	ros2bag mcap zstd	18.10	43.99 / 106.00	115.93 / 118.03	18.99	1.05	1	15,146

directly as per-day SQLite files (gps/YYYY-MM-DD.sqlite3) using the avs\_gps schema.

When the archive service is invoked (e.g., ./archive -before YYYY/MM/DD), each daily directory for images and LiDAR is first packed into a single .tar file to reduce fragmentation and improve sequential I/O efficiency, then relocated to the HDD. The HDD is organized by year and month (archive image(or lidar)/YYYY/MM/YYYY-MM-DD.tar to avoid overly deep directories as the dataset grows. Archival catalog tables archive\_image and archive\_lidar record, for each tarball, its begin and end timestamps, file count or row count for GPS data, and archive time, enabling precise lookup and management. GPS per-day databases are moved directly to archive\_gps/YYYY/MM/YYYY-MM-DD.sqlite3, with the archive table of gps updated accordingly. The complete hot and cold schemas are shown in Figure 10. After a successful archive commit (files moved and archive databases updated), the corresponding SSD files and index entries are removed to preserve SSD lifespan, while the HDD remains the authoritative cold storage tier.

#### **6.2** System Performance

The performance of AVS is evaluated over three days of repeated city-route drives (11–12 minutes each) on a Lincoln MKZ based L4 autonomous vehicle platform, shown in Figure 11. The workload includes mix and concurrent data stream of 10 Hz Hesai Pandar64 LiDAR (sensor\_msgs/PointCloud2), 10 Hz Basler Ace mono8 images (sensor\_msgs/Image), and 50 Hz NovAtel OEM7 GNSS (gps\_msgs/GPSFix).

**Recording.** The first experiment compares AVS with four ros2bag modes: SQLite, SQLite+Zstd, MCAP, and MCAP+Zstd. Table 8 reports data growth, CPU/memory usage, and NVMe SMART counters.

AVS shrinks logs to 4.0 GB on average, compared to 33.8



Figure 11: L4 autonomous driving platform and AVS prototype.

GB for SQLite or MCAP raw, and 19.9 GB for per-message Zstd compression modes, which are  $8.4 \times$  and  $5.0 \times$  smaller, respectively. Device wear is best captured by the write amplification factor (WAF) and total bytes written; although AVS shows a higher WAF due to many small fsyncs, its absolute device writes are far lower. AVS also generates more host write commands (hundreds of thousands vs. tens of thousands), yet controller busy time remains similar. Overall, AVS trades CPU and memory for order-of-magnitude storage savings and reduced wear. At the same time, MCAP's log-append structure, which minimizes host write commands, suggests a promising direction for future AVS design.

Table 9 shows that ingest remains comfortably real-time: even p99 latencies fall within 10Hz/50Hz budgets. Tails are tight (small p50–p99 gaps) with no queue growth. Peak permodule RSS is modest (113/54/31 MB) and non-overlapping, matching the  $\approx 200$  MB process RSS in Table 8. Overall, the results demonstrate bounded latency tails and stable memory usage while shrinking bytes before they reach disk.

**Archiving Benchmark.** The archiving stage was evaluated on the stored three-day dataset over 10 runs, measuring CPU and memory usage, end-to-end latency, and final archive size, as shown in Table 10. The results show that archiving is

Table 9: AVS ingest performance.

Modality	Peak RSS (MB)	p50 (ms)	p95 (ms)	p99 (ms)
Image	113.26	25.76	29.05	29.71
LiDAR	53.74	50.87	59.54	60.99
GPS	30.62	0.74	1.00	1.58

Table 10: AVS archive performance over 10 runs.(Total archive data size is 12554.14 MB)

	CPU (%)	RSS (MB)	Latency (s)
Maximum	100.44	14.47	157.35
Average	24.05	13.10	143.99
95% CI	$\pm 1.16$	$\pm 0.17$	$\pm 7.14$

lightweight, with modest average resource use, tight variability, and predictable tails. Because this process can be scheduled during off-peak periods (e.g., overnight), large batches of logs can be compacted and migrated with low interference to the system. This enables AVS to sustain long-term retention by periodically moving hot SSD data into efficient HDD archives while preserving real-time ingest and query performance.

**Retrieve Usage.** To illustrate the advantages of AVS beyond storing, We evaluate AVS's end-to-end retrieval on the whole trace. For each modality (image, lidar, gps), we enumerate items in the specified time range, sample N=6 random 75 s windows (fixed seed;  $\geq 2$  items/window), align window boundaries to minute granularity to measure startup latency: Time To First Byte(TTFB) and steady-state per-item decode latency. We aggregate across windows and report the results per modality for both metrics in Table 11.

LiDAR starts fastest with tight tails; images start slightly slower but have similarly steady per-item decode. GPS is effectively instant. The small p50 to p99 gaps across modalities indicate low tail latency and predictable replay.

**Observation 3: Memory pressure.** AVS applies permodality reduction/compression pre-persistence; image dedup briefly holds a working copy, inflating peak RSS. As streams and rates scale, peak RSS grows roughly with concurrent codecs and pipelines. Open questions include: Is there a bounded-memory ingest algorithm that could keep peak RSS = O(# streams) with small constants using streaming codecs (short windows) or chunked pipelines that avoid duplicate working sets? Alternatively, can we develop a budgeted adaptation that adjusts the memory budget controller to increase reduction levels (larger voxel size, lower JPEG quality) when RSS thresholds are exceeded, while maintaining stable ingest p99?

**Observation 4: SSD endurance.** Our ingest produces many small files with durability (fsync) across multiple sensors. The reported results indicate that we meet real-time bud-

Table 11: AVS retrieval performance.

	TTFB (ms)			Per-item latency (ms)		
Modality	p50	p95	p99	p50	p95	p99
image	29.2483	29.4701	29.4898	20.3396	21.0217	21.2118
lidar	23.3854	26.5466	26.8276	20.1891	22.2782	23.6313
gps	0.5661	0.5781	0.5791	0.0003	0.0003	0.0057

gets; however, we did not instrument device-internal effects. Open questions include: Would batching durability, such as group-commit over N files and preallocating to erase-block-friendly extents, reduce tail latency? Does a log-structured layout (append-only per-sensor extents with metadata indexing) outperform file-per-scan without harming retrieval? These require further testing with richer SMART/NVMe counters, direct fsync tail-latency tracing, and controlled small-write stress experiments.

#### 7 Conclusion and Future Work

The paper tackles the challenge that autonomous vehicles lack a general-purpose, queryable on-board storage system for massive, heterogeneous sensor streams that vehicle computing and future data-driven applications rely on. Existing loggers and storage stacks fall short in efficient storage, selective retrieval, and economical long-term retention under edge constraints. To bridge this gap, the work introduces AVS, a computational and hierarchical storage architecture that treats storage as a first-class component in the AV stack.

AVS brings three core innovations. First, it applies useguided, modality-aware reduction for unstructured data at ingest: 0.2 m voxel downsampling cuts LiDAR storage to 24% of the original; perceptual-hash deduplication retains 72% of image frames; and fit-for-purpose codecs LAZ and JPEG shrink data with 6.56 and 4.06 compression ratios, respectively, while preserving downstream utility. Second, it organizes storage into a hot—cold hierarchy: a hot SSD tier for line-rate ingest and low-latency queries, complemented by an HDD archival tier tuned for sequential writes and long-term retention, with the use of XFS filesystem that keeps tar archives contiguous with no observed fragmentation, and to sustain higher throughput. Finally, it integrates a lightweight SQLite-based index that supports efficient, query-friendly access under tight compute constraints.

Prototype evaluation on a Raspberry Pi 5 with three days of real L4 autonomous driving traces validated this design. It demonstrates predictable ingest within 10 Hz/50 Hz budgets, fast selective retrieval (time-to-first-byte is around 29 ms for images, 23 ms for LiDAR, 0.6 ms for GPS), and substantial footprint reductions, on average 8.4× versus raw ros2bag and 5.0× versus ros2bag with zstd compression.

In summary, AVS shows that first-class on-vehicle storage is not only feasible but necessary, delivering predictable

ingest, efficient retrieval, and principled reduction. It also reveals a characteristic I/O profile that should shape future designs: write-heavy ingest, small random reads for queries, and long sequential scans. Collectively, the paper's four observations and accompanying open questions establish a foundation for the next wave of vehicle data-driven applications and motivate deeper exploration of storage design in autonomous systems.

#### Acknowledgments

This work is funded by the US National Science Foundation (NSF) under Grant NSF/CNS 2231523.

#### References

- [1] Rashid Abbasi, Ali Kashif Bashir, Hasan J. Alyamani, Farhan Amin, Jaehyeok Doh, and Jianwen Chen. Lidar point cloud compression, processing and learning for autonomous driving. *IEEE Transactions on Intelligent Transportation Systems*, 24(1):962–979, 2023.
- [2] Jan-Aike Bolte, Andreas Bar, Daniel Lipinski, and Tim Fingscheidt. Towards corner case detection for autonomous driving. In 2019 IEEE Intelligent vehicles symposium (IV), pages 438–445. IEEE, 2019.
- [3] Holger Caesar, Varun Bankiti, Alex H. Lang, Sourabh Vora, Venice Erin Liong, Qiang Xu, Anush Krishnan, Yu Pan, Giancarlo Baldan, and Oscar Beijbom. nuscenes: A multimodal dataset for autonomous driving. In *CVPR*, 2020.
- [4] Hongming Cai, Boyi Xu, Lihong Jiang, and Athanasios V Vasilakos. Iot-based big data storage systems in cloud computing: perspectives and challenges. *IEEE Internet of Things Journal*, 4(1):75–87, 2016.
- [5] Andreas Geiger, Philip Lenz, Christoph Stiller, and Raquel Urtasun. Vision meets robotics: The kitti dataset. *International Journal of Robotics Research* (*IJRR*), 2013.
- [6] Google. WebP: An image format for the web. https: //developers.google.com/speed/webp, 2010. Accessed: 2025-02-15.
- [7] Harshit Gupta and Umakishore Ramachandran. Fogstore: A geo-distributed key-value store guaranteeing low latency for strongly consistent access. In *Proceed*ings of the 12th ACM International Conference on Distributed and Event-based Systems, pages 148–159, 2018.
- [8] Martin Isenburg. Laszip: lossless compression of lidar data. *Photogrammetric engineering and remote sensing*, 79(2):209–217, 2013.

- [9] Shehbaz Jaffer, Stathis Maneas, Andy Hwang, and Bianca Schroeder. Evaluating file system reliability on solid state drives. In 2019 USENIX Annual Technical Conference (USENIX ATC 19), pages 783–798, 2019.
- [10] Fiodar Kazhamiaka, Matei Zaharia, and Peter Bailis. Challenges and opportunities for autonomous vehicle query systems. In CIDR, 2021.
- [11] Liangkai Liu, Sidi Lu, Ren Zhong, Baofu Wu, Yongtao Yao, Qingyang Zhang, and Weisong Shi. Computing systems for autonomous driving: State of the art and challenges. *IEEE Internet of Things Journal*, 8(8):6469–6486, 2020.
- [12] Sidi Lu and Weisong Shi. Vehicle computing: Vision and challenges. *Journal of Information and Intelligence*, 1(1):23–35, 2023.
- [13] Luís Manuel Meruje Ferreira, Fabio Coelho, and José Pereira. Databases in edge and fog environments: A survey. *ACM Computing Surveys*, 56(11):1–40, 2024.
- [14] Jayashree Mohan, Rohan Kadekodi, and Vijay Chidambaram. Analyzing io amplification in linux file systems. *arXiv preprint arXiv:1707.08514*, 2017.
- [15] National Highway Traffic Safety Administration. Event data recorders; final rule. Federal Register, 89 FR 93741, 2024. Amends 49 CFR Part 563 to extend timed data recording from 5 s@2 Hz to 20 s@10 Hz.
- [16] Adrian-Cristian Nicolaescu, Spyridon Mastorakis, and Ioannis Psaras. Store edge networked data (send): A data and performance driven edge storage framework. In IEEE INFOCOM 2021-IEEE Conference on Computer Communications, pages 1–10. IEEE, 2021.
- [17] Radu Bogdan Rusu and Steve Cousins. 3d is here: Point cloud library (pcl). In 2011 IEEE International Conference on Robotics and Automation, pages 1–4, 2011.
- [18] Pei Sun, Henrik Kretzschmar, Xerxes Dotiwalla, Aurelien Chouard, Vijaysai Patnaik, Paul Tsui, James Guo, Yin Zhou, Yuning Chai, Benjamin Caine, Vijay Vasudevan, Wei Han, Jiquan Ngiam, Hang Zhao, Aleksei Timofeev, Scott Ettinger, Maxim Krivokon, Amy Gao, Aditya Joshi, Yu Zhang, Jonathon Shlens, Zhifeng Chen, and Dragomir Anguelov. Scalability in perception for autonomous driving: Waymo open dataset. In *Proceedings of the IEEE/CVF Conference on Computer Vision and Pattern Recognition (CVPR)*, June 2020.
- [19] David Taubman. High performance scalable image compression with ebcot. *IEEE Transactions on image processing*, 9(7):1158–1170, 2000.

- [20] Andreas Theissler, Judith Pérez-Velázquez, Marcel Kettelgerdes, and Gordon Elger. Predictive maintenance enabled by machine learning: Use cases and challenges in the automotive industry. *Reliability engineering & system safety*, 215:107864, 2021.
- [21] Andreas Venus, Giulietta Poltronieri, Marc de Jong, and Martin Kellner. The rise of edge ai in automotive. McKinsey & Company, August 2025. Accessed: 2025-09-11.
- [22] Ignacio Vizzo, Tiziano Guadagnino, Benedikt Mersch, Louis Wiesmann, Jens Behley, and Cyrill Stachniss. Kiss-icp: In defense of point-to-point icp-simple, accurate, and robust registration if done the right way. *IEEE Robotics and Automation Letters*, 8(2):1029–1036, 2023.
- [23] Gregory K Wallace. The jpeg still picture compression standard. *Communications of the ACM*, 34(4):30–44, 1991.
- [24] Ruijun Wang, Liangkai Liu, and Weisong Shi. Hydraspace: Computational data storage for autonomous vehicles. In 2020 IEEE 6th International Conference on Collaboration and Internet Computing (CIC), pages 70–77. IEEE, 2020.
- [25] Yuxin Wang, Yuankai He, Ruijun Wang, and Weisong Shi. Quantitative analysis of storage requirement for autonomous vehicles. In *Proceedings of the 16th ACM Workshop on Hot Topics in Storage and File Systems*, pages 71–78, 2024.
- [26] Xin Xia, Zonglin Meng, Xu Han, Hanzhao Li, Takahiro Tsukiji, Runsheng Xu, Zhaoliang Zheng, and Jiaqi Ma. An automated driving systems data acquisition and analytics platform. *Transportation research part C: emerging technologies*, 151:104120, 2023.
- [27] Zijun Xu, Xuanjun Wen, Yanjie Song, and Shu Yin. Rosfs: A user-level file system for ros. *arXiv preprint arXiv:2406.10635*, 2024.
- [28] Hang Yin and Christian Berger. When to use what data set for your self-driving car algorithm: An overview of publicly available driving datasets. In 2017 IEEE 20th International Conference on Intelligent Transportation Systems (ITSC), pages 1–8. IEEE, 2017.
- [29] Christoph Zauner. Implementation and benchmarking of perceptual image hash functions. 2010.
- [30] Xingyi Zhou, Vladlen Koltun, and Philipp Krähenbühl. Tracking objects as points. *ECCV*, 2020.